PCCP

Accepted Manuscript

ROYAL SOCIETY OF CHEMISTRY

www.rsc.org/pccp

Journal Name

RSCPublishing

ARTICLE

Predicting suitable optoelectronic properties of monoclinic VON semiconductor crystals for photovoltaics using accurate first-principles computations

Cite this: DOI: 10.1039/xoxxoooooox

Received ooth January 2012,
Accepted ooth January 2012

DOI: 10.1039/xoxxoooooox

www.rsc.org/

Moussab Harb*

Using accurate first-principles quantum calculations based on DFT (including the perturbation theory DFPT) with the range-separated hybrid HSE06 exchange-correlation functional, I predict essential fundamental properties (such as bandgap, optical absorption coefficient, dielectric constant, charge carrier effective masses and exciton binding energy) of two stable monoclinic vanadium oxynitride (VON) semiconductor crystals for solar energy conversion applications. In addition to the predicted band gaps in the optimal range for making single-junction solar cells, both polymorphs exhibit relatively high absorption efficiencies in the visible range, high dielectric constants, high charge carrier mobilities and much lower exciton binding energies than the thermal energy at room temperature. Moreover, their optical absorption, dielectric and exciton dissociation properties are found to be better than those obtained for semiconductors frequently utilized in photovoltaic devices like Si, CdTe and GaAs. These novel results offer a great opportunity for this stoichiometric VON material to be properly synthesized and considered as a new good candidate for photovoltaic applications.

1. Introduction

Harvesting solar energy into electricity using semiconductor materials is a real opportunity for sustainable development at low environmental and economic costs.[1-5] In addition to the high crystallinity needed for the developed material, three challenging fundamental requirements must be simultaneously justified in the semiconductor as a photon absorber for achieving efficient solar energy conversion: (i) the bandgap energy must be in the 1.1-1.4 eV range which represents the optimum zone known for a maximum efficiency;[6] (ii) the static dielectric constant must be higher than 10 and the exciton binding energy must be lower than 25 meV (thermal energy at room temperature) to obtain an efficient dissociation of the photogenerated exciton into free charge carriers;[7-12] (iii) the charge carrier effective masses must be smaller than $0.5\,m_0$ (m_0 is the free electron mass) to obtain good charge carrier transport properties.[7,13,14] Besides, the photogenerated holes and electrons must migrate through two different crystallographic directions to efficiently help for the required separation of the charge carriers at the surface of the semiconductor.

Nowadays, the density functional theory (DFT) can greatly help the experimentalists for a rational design of new semiconductors for solar energy applications by computing these fundamental properties since some of them are quite difficult to be obtained experimentally. The accuracy of DFT calculations, which is highly required here, is directly linked to the quality of the functional used to describe the various electronic exchange and correlation interactions.

In previous theoretical studies reported on the electronic structures and optical absorption properties of metal oxide-, oxynitride- and nitride-based semiconductors,[15-23] I have shown that the use of DFT (including the perturbation theory DFPT) along with the range-separated hybrid (HSE06) exchange-correlation functional yield much more accurate bandgap and optical transition predictions than standard DFT calculations as compared with the experimental data. In addition, I show in Tables 1-4 that my computed bandgaps, dielectric constants, charge carrier effective masses and exciton binding energies of widely used semiconductors in photovoltaic solar cells such as Si, CdTe and GaAs with HSE06 accurately reproduce the experimental data.[24]

Recently, I have investigated by DFT the optoelectronic features of monoclinic TaON compound and demonstrated good exciton disscociation ability and good charge carrier transport properties using this material.[23] Nevertheless, the predicted bandgap was quite large (3.0 eV) which indicates that this compound can only absorb the UV light.

Table 1 Computed bandgaps (in eV) of Si, CdTe, and GaAs using HSE06. The calculated values are compared to experimental data.

solid	structure	HSE06	Expt.
Si	diamond	1.23	1.17[7]
CdTe	zincblende	1.56	1.50[7]
GaAs	zincblende	1.68	1.52[13]

Table 2 Computed high-frequency (ε_∞) and static (ε_r) dielectric constants of Si, CdTe, and GaAs using HSE06. The calculated values are compared to experimental data.

Solid	structure	ε_∞		ε_r	
		HSE06	Expt.	HSE06	Expt.
Si	diamond	11.8	12.1[7]	11.8	12.1[7]
CdTe	zincblende	7.4	7.1[7]	10.4	10.4[7]
GaAs	zincblende	12.3	10.8[8]	14.6	13.0[8]

Table 3 Computed effective masses of holes (m_h^*) and electrons (m_e^*) of Si, CdTe, and GaAs using HSE06 (m_0 is the free electron mass). The calculated values are compared to experimental data. The symbols ⊥ and || mean the transverse and longitudinal directions, respectively, while (h) and (l) mean heavy and light holes.

Solid	structure	m_h^*/m_0		m_e^*/m_0	
		HSE	Expt.	HSE	Expt.
Si	diamond	0.37 0.11	0.54(h)[7] 0.15(l)[7]	0.11 0.79	0.19(⊥)[7] 0.92(||)[7]
CdTe	zincblende	0.17 0.78	0.12(l)[7] 0.81(h)[7]	0.1	0.09[7]
GaAs	zincblende	0.5 0.12	0.55(h)[14] 0.08(l)[14]	0.09	0.07[13]

Table 4 Computed exciton binding energy (in meV) of Si, CdTe, and GaAs using HSE06. The calculated values are compared to experimental data.

solid	structure	HSE06	Expt.
Si	diamond	15.6	15[9]
CdTe	zincblende	10	10[11]
GaAs	zincblende	3.8	5[12]

These theoretical results ignited my interests to carry out a detailed DFT study on the optoelectronic properties of monoclinic vanadium oxynitride (VON) crystal in order to predict its ability for solar energy conversion. Hence, I applied the accurate first-principles quantum methodology mentioned above to systematically investigate the electronic structure, optical absorption properties, dielectric constant tensor, charge carrier effective mass tensors and exciton binding energy of this material. I systematically compared my calculated results with those obtained for semiconductors widely utilized in photovoltaic solar cells like Si, CdTe and GaAs. To the best of my knowledge, there is no previous experimental or DFT report (using this level of theory) of a systematic study on the photophysical properties of the stoichiometric VON material.

2. Computational methods

2.1. Structure relaxation and formation energy calculations

For the simulation of VON structure, I considered the two common monoclinic crystalline phases of TaON (or NbON) identified experimentally by neutron powder diffraction technique.[25,26] I followed here the pressure-homologue rule of Neuhaus stating that, under pressure, a compound adapts the structure of its higher homologues.[27] The crystal structures of these two materials (including those for Si, CdTe and GaAs) were fully optimized by DFT implemented in VASP program[28-31] with the PBE exchange-correlation functional[32] and the Projector-Augmented Plane Wave (PAW) approach.[33] The valence atomic configurations used in the calculations were $3p^6 3d^4 4s^1$ for V, $2s^2 2p^4$ for O, $2s^2 2p^3$ for N, $3s^2 3p^2$ for Si, $5s^2 4d^{10}$ for Cd, $5s^2 5p^4$ for Te, $4s^2 4p^1$ for Ga and $4s^2 4p^3$ for As. The Brillouin zones of β- and γ-VON crystalline phases were sampled with 6 × 6 × 6 and 3 × 10 × 6 Monkhorst-Pack *k*-point grid,[34] respectively. For Si, CdTe and GaAs, the Brillouin zone was sampled with 5 × 5 × 5 *k*-point mesh. The ionic coordinates and cell parameters were fully relaxed (residual force components below 0.01 eV Å). The convergence criterion for the self-consistent cycles was fixed at 10^{-5} eV. My computed cell parameters for Si, CdTe and GaAs revealed an excellent agreement with the available experimental data (Table S1, ESI†). The atomic positions of V, O and N in the relaxed β- and γ-VON structures are given in Tables S2 and S3 (ESI†).

The thermodynamic stability of VON was computed by assembling this material from individual elements using the following expression:

$$E_{form} = E_{tot}(VON) - E_{tot}(V) - \tfrac{1}{2}E_{tot}(O_2) - \tfrac{1}{2}E_{tot}(N_2) - \Delta\mu_O - \Delta\mu_N \quad (1)$$

It includes the total energies at 0 K of VON and V solids in their ground-state structures and of gas phase O_2 and N_2 molecules. $\Delta\mu_O$ and $\Delta\mu_N$ are the chemical potentials of oxygen and nitrogen that depend on the temperature (*T*) and pressure (*p*) *via* the enthalpy (*h*) and entropy (*s*) corrections of each gas phase molecule as follows:

$$\Delta\mu_{O,N} = h_{O_2,N_2}(T) - Ts_{O_2,N_2}(T) + RTLn\left(\frac{p(O_2,N_2)}{p_0}\right) \quad (2)$$

The enthalpy and entropy corrections as a function of *T* were obtained from DMol[35] using PBE functional and DNP basis set.[36] All electronic energies were calculated using VASP program. In what follows, I fixed $\Delta\mu_O$ and $\Delta\mu_N$ at -0.22 and -0.18 eV, respectively, for T = 298 K and $p(O_2) = p(N_2)$ = 1 atm (standard thermodynamic conditions). Negative or positive formation energy corresponds to stable or unstable material.

2.2. Electronic structure and UV-visible optical absorption calculations

For electronic density-of-state and *k*-space band-structure calculations, I employed the range-separated hybrid HSE06[37]

exchange-correlation functional implemented in VASP.[28-31] The tetrahedron method with Bloch corrections for the Brillouin zone integration was used for density of states whereas Gaussian smearing was adopted for energy dispersions curves.

For UV-visible optical absorption calculations, I applied the density functional perturbation theory (DFPT) implemented in VASP[28-31] by employing the HSE06 functional.[37] The optical properties were determined through the frequency-dependent complex dielectric following a methodology described in these references.[38-40] The optical absorption coefficient (in cm^{-1}) of the solid was then computed using the formula:

$$\alpha(\omega) = (4\pi/\lambda)k(\omega) \quad (3)$$

where λ and ω are the wavelength and the frequency of the incident light, and $k(\omega)$ is the imaginary component of the complex refractive index or the extinction coefficient which was computed using the expression:

$$k(\omega) = \{[(\varepsilon_1^2 + \varepsilon_2^2)^{1/2} - \varepsilon_1]/2\}^{1/2} \quad (4)$$

$\varepsilon_1(\omega)$ and $\varepsilon_2(\omega)$ are the real and imaginary parts of the dielectric function averaged over the three polarization vectors, respectively. $\varepsilon_1(\omega)$ was calculated using the Kramers-Kronig relation. $\varepsilon_2(\omega)$ was calculated by summing all the possible transitions from occupied to unoccupied states in the Brillouin zone weighted with the matrix element describing the probability of transition.

2.3. Dielectric constant, charge carrier effective masses and exciton binding energy calculations

The electronic contribution (ε_∞) to the static dielectric constant tensor was computed from the self-consistent response of the crystal to a finite electric field[41] implemented in VASP[28-31] using the HSE06 functional.[37] This is a perturbative method which includes the local field effects and focuses on the description of the relaxation of crystalline orbitals under the effect of an external static electric field. A good description of the bandgap generally leads to a good description of ε_∞. The ionic contribution (ε_{vib}) was obtained by computing the full phonon spectrum of the crystal using DFPT within the linear response method implemented in VASP and the PBE functional. Finally, the macroscopic static dielectric constant tensor (ε_r) was defined by the sum of both electronic and ionic contributions as follows:

$$\varepsilon_r = \varepsilon_\infty + \varepsilon_{vib} \quad (5)$$

The effective mass tensors of photogenerated holes (m_h^*) and electrons (m_e^*) at the band edges of these compounds were computed on the basis of their *k*-space band structure obtained from HSE06 using the following relation:

$$\left(\frac{1}{m^*}\right)_{ij} = \frac{1}{\hbar^2}\frac{\partial^2 E_n(k)}{\partial k_i k_j}(i,j = x,y,z) \quad (6)$$

where *i* and *j* denote reciprocal components and $E_n(k)$ is the dispersion relation for the *n*-th band. Note that the derivatives were evaluated numerically using the finite difference method.[42]

The exciton binding energy (E_b) was then estimated from the hydrogenic model[43] using the formula:

$$E_b = \frac{\mu}{m_0 \varepsilon_r^2} R_H \quad (7)$$

where R_H is the Rydberg constant of the hydrogen atom (13.6 eV), m_0 is the free electron mass and μ is the effective reduced mass of the exciton which is given by:

$$\frac{1}{\mu} = \frac{1}{m_h^*} + \frac{1}{m_e^*} \quad (8)$$

For the cubic structures, the effective masses of the electron and the hole were taken as the arithmetic mean of the components in the three crystallographic directions, while the geometric mean was adopted for the non-cubic structures. In all types of structures, the dielectric constant was obtained from the arithmetic mean of the components in the three crystallographic directions.

3. Results and discussion

3.1. Structural characterization and energetics

Fig. 1 illustrates the two crystal structures considered for VON. Their calculated formation energies (at 298 K, 1 atm) together with the lattice parameters and the various bond lengths are reported in Table 5. The β-phase exhibits a monoclinic crystal lattice (space group $P2_1/c$) and its structure is formed by edge-sharing irregular VO_3N_4 polyhedral species (Fig. 1a) with V-O bond lengths ranging from 1.80 to 2.03 Å and V-N bond lengths ranging from 1.95 to 2.04 Å. For γ-phase, the crystal lattice is also monoclinic (space group *C2/m*) and the structure is composed of corner- and edge-sharing regular VO_3N_3 and VO_2N_4 octahedral species with V-O bond lengths ranging from 1.69 to 1.91 Å and V-N bond lengths ranging from 1.68 to 2.01 Å (Fig. 1b). The calculated formation energies of both structures are found to be negative with -3.52 eV for β-phase and -3.77 eV for γ-phase, and so, both crystal structures are likely to be stable.

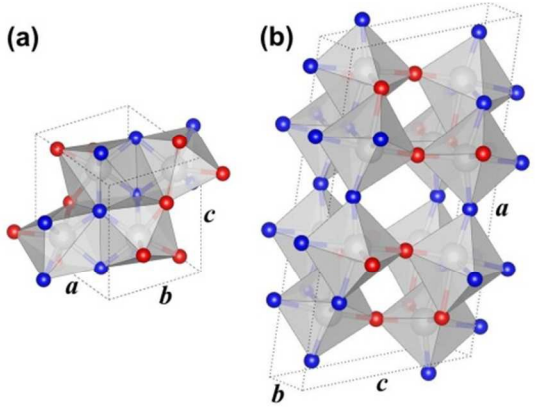

Fig. 1 DFT-optimized crystal structures of (a) β-VON and (b) γ-VON phases. Color legend: V in gray, O in red, N in blue. The rigid frameworks represent the VO_3N_4 polyhedral, VO_3N_3, and VO_2N_4 octahedral species in the structures.

Journal Name RSCPublishing

ARTICLE

Table 5 Computed formation energies (at 298 K, 1 atm) of the two optimized VON structures using PBE together with the lattice constants and bond lengths.

structure	formation energy (eV)	lattice constants						bond lengths	
		a (Å)	*b* (Å)	*c* (Å)	*α* (º)	*β* (º)	*γ* (º)	V-O (Å)	V-N (Å)
β-VON (1a)	-3.52	4.73	4.71	4.92	89.9	99.2	90	1.80/2.03	1.95/2.04
γ-VON (1b)	-3.77	12.22	3.63	6.35	90	107.1	90	1.69/1.91	1.68/2.01

3.2. Bandgap and solar energy absorption efficiency: comparison with Si, CdTe and GaAs

The calculated electronic densities of states (DOS) and energy dispersion diagrams of β- and γ-VON structures using HSE06 are shown in Fig. 2. For β-phase, the valence band states located within 1.2 eV range below the Fermi level are made by mixtures of N 2p and Ta5d orbitals with weak contributions from O 2p orbitals, while the conduction band states are mainly composed of empty V 5d orbitals (Fig. 2a). My calculations predict this compound to be a direct (at the Γ point) semiconductor with small bandgap energy of 1.4 eV. In the case of γ-phase, the analysis reveals a valence bandwidth within 0.4 eV range below the Fermi level which is dominated by occupied N 2p orbitals with weak contributions from O 2p and Ta 5d orbitals whereas the lower part is found to be governed by occupied O 2p states, in line with the lower electronegativity of O with respect to N (Fig. 2b). The conduction band of this compound primarily consists of empty V 5d orbitals. This material is also predicted as a direct (at the Γ point) semiconductor with small bandgap energy of 1.3 eV. The lowest-energy band gap of this compound originates from direct N $2p^6$-V $5d^0$ orbital transitions. Note that I checked the spin-orbit coupling effect on the electronic structures of both phases and no bandgap change was found.

In order to study the solar energy harvesting properties of β- and γ-VON structures, I have calculated the optical absorption coefficient of each of them as a function of the wavelength of incident light through the imaginary and real parts of the dielectric function computed using HSE06 following the methodology described in the computational methods section. As shown in Fig. 3, the two calculated absorption spectra exhibit roughly similar behavior revealing the appearance of high-intensity absorption features in the visible range with broad edges extending up to 800 nm. Interestingly, if I compare my calculated spectra with those obtained for Si, CdTe and GaAs, I can see that the absorption efficiencies of both VON crystals are much higher than Si and CdTe in the entire visible-light range, and superior to that obtained for GaAs in the blue region, as shown in Fig. 3. This result clearly indicates that the monoclinic VON bulk crystal can be considered as good solar energy absorber in the visible light spectrum.

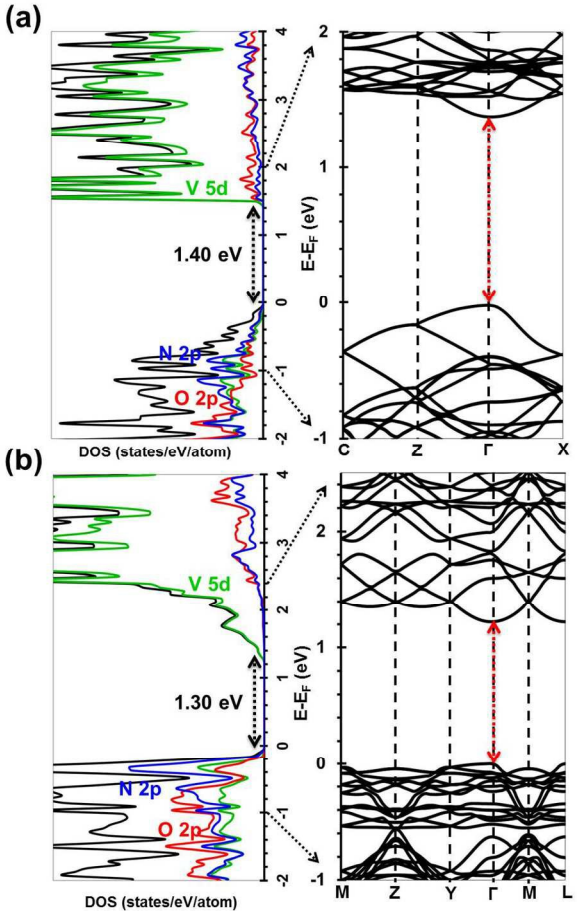

Fig. 2 Electronic densities of states (DOS) and band dispersions of (a) β-VON and (b) γ-VON structures computed using HSE06. Color legend: total DOS in black, projected DOS on V 5d orbitals in green, on O 2p orbitals in red, and on N 2p orbitals in blue. Fermi level is set at 0 eV.

Journal Name RSCPublishing

ARTICLE

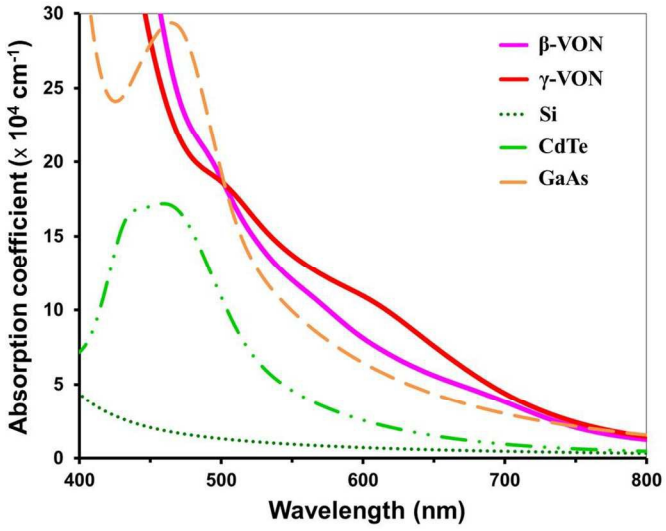

Fig. 3 Optical absorption spectra of β- and γ-VON structures computed using HSE06. The calculated spectra are compared with those of Si, CdTe, and GaAs in the visible range.

3.3. Exciton dissociation ability and charge carrier transport properties: comparison with Si, CdTe and GaAs

I have calculated the high-frequency (electronic contribution) and static (electronic and ionic contributions) dielectric constant tensors of those crystals using PBE and HSE06 functionals following the methodology described in the computational methods section. My computed components in the three principal crystallographic directions are reported in Table 6. In the case of β-phase, I found high static (ε_r) dielectric constants (> 10) with values of 35.0, 49.6, and 33.4 along [001], [010], and [001] directions, respectively, and an average value of 39.3. For γ-phase, higher static dielectric constants of 35.9, 52.1, and 51.4 were obtained along the three principal directions with an average value of 46.4. Importantly, the major contribution to the static dielectric constant in both cases comes from the ionic component which reveals the strong ionic character of the crystal. This is mainly due to the high electronegativity of oxygen which yields important Born charges in the material. My calculated dielectric constants for both VON phases are much higher than those calculated for Si (which is 12.1), for CdTe (which is 10.4) and for GaAs (which is 14.6). This suggests excellent dielectric properties of VON compound which should be much better than those for Si, CdTe and GaAs.

To gain insight into the charge carrier transport properties of β- and γ-VON structures, I have computed the effective masse tensors of photogenerated holes and electrons at their band edges (see the computational methods section for more details) using the *k*-space electronic band structures obtained from HSE06. My calculated values in the three principal directions reveal important anisotropies in both cases, as shown in Table 6. For β-VON structure, the hole effective masses along [010] and [001] directions are found to be relatively small (< $0.5\,m_0$) while a much larger value than $0.5\,m_0$ was obtained along [100] direction. In contrast, small electron effective masses (< $0.5\,m_0$) were found along the three principal directions. Consequently, good electron transport properties are expected in the three directions whereas the hole mobilities are expected to be good along [010] and [001 directions but very low in [100] direction. In the case of γ-VON structure, both hole and electron effective masses are found to be relatively small (< $0.5\,m_0$) along [010] and [001] directions, and therefore, good charge carrier transport properties are expected in the *bc* plane. Nevertheless, large values (> $0.5\,m_0$) were obtained along [100] direction, and so low charge carrier mobilities are expected in this specific direction. Interestingly, the photogenerated holes and electrons in both phases have the possibility to migrate very easily through two different crystallographic directions, and so efficient charge carrier separation is expected at the surfaces of these two compounds. My smallest calculated charge carrier effective masses for both β-VON (which are $m_h^* = 0.18\,m_0$; $m_e^* = 0.12\,m_0$) and γ-VON (which are $m_h^* = 0.28\,m_0$; $m_e^* = 0.10\,m_0$) structures are very close to those calculated for Si (which are $m_h^* = 0.11\,m_0$; $m_e^* = 0.11\,m_0$), for CdTe (which are $m_h^* = 0.17\,m_0$; $m_e^* = 0.10\,m_0$) and for GaAs (which are $m_h^* = 0.12\,m_0$; $m_e^* = 0.09\,m_0$). This should yield high charge carrier mobilities in the VON material similarly as invoked in the case of Si, CdTe and GaAs.

Finally, I have evaluated the exciton dissociation ability into free charge carriers using both VON crystalline phases by computing the exciton binding energy (E_b) through the hydrogenic model (see the computational methods for more details) and the HSE06 functional. Very low values of 1.4 and 1.0 were obtained for β- and γ-structures, respectively. It is important to stress that my calculated exciton binding energies are found to be much lower than 25 meV (which is thermal energy at room temperature), and this should lead to an efficient exciton dissociation into free charge carriers using this material. As these calculated values are much lower than those calculated for Si (which is 15.6 meV), for CdTe (which is 10 meV) and for GaAs (which is 3.8 meV), the exciton dissociation ability is expected to be much easier using VON than Si, CdTe and GaAs.

Journal Name RSCPublishing

ARTICLE

Table 6 Computed optical (ε_∞) and static (ε_r) dielectric constants and effective masses of holes (m_h^*) and electrons (m_e^*) in the three principal directions of β- and γ-VON structures using HSE06. m_0 is the free electron mass.

	ε_∞		ε_r		m_h^*/m_0		m_e^*/m_0	
	β-phase	γ-phase	β-phase	γ-phase	β-phase	γ-phase	β-phase	γ-phase
[100]	18.0	15.2	35.0	35.9	2.58	0.82	0.24	1.19
[010]	22.1	19.1	49.6	52.1	0.40	0.28	0.12	0.20
[001]	19.2	12.5	33.4	51.4	0.18	0.29	0.26	0.10

4. Conclusion

By applying accurate first-principles quantum calculations based on DFT (including the perturbation approach DFPT) within the range-separated hybrid HSE06 exchange-correlation functional, I have investigated essential fundamental properties of vanadium oxynitride (VON) semiconductor compound within two different stable monoclinic crystal structures to predict its ability for solar energy conversion. The formation energy, electronic structure, optical absorption response, dielectric constant, charge carrier effective masses and exciton binding energy were systematically computed for both crystalline phases. My calculations predicted both VON polymorphs to be semiconductors with small direct bandgaps in the 1.3-1.4 eV range which is known to be the optimum zone for a maximum efficiency. In addition, I showed that both crystals exhibit high absorption efficiencies in the visible range, high dielectric constants (> 10), small charge carrier effective masses (< 0.5 m_0) along two different crystallographic directions and low exciton binding energies (< 25 meV). Their optical absorption, dielectric and exciton dissociation properties were found to be better than those obtained for widely used semiconductors in photovoltaic solar cells such as Si, CdTe and GaAs. Therefore, these novel results will certainly offer a grand opportunity for this stoichiometric and crystalline VON material to be properly synthesized and considered as a new good candidate for photovoltaic applications. The computational approach adopted in this study showed high accuracy in the prediction of optoelectronic properties originated from the precise calculation of the electronic structure. This advanced and robust first-principle quantum methodology described in this study will definitely be applied to identify good candidate materials among novel semiconductor compounds for a large variety of technological interests.

Acknowledgements

This research work was supported by King Abdullah University of Science and Technology (KAUST). The author gratefully thanks the High Performance Computing department (HPC) at KAUST for the computational time attributed to this project.

Notes and references

Division of Physical Sciences and Engineering, KAUST Catalysis Center (KCC), King Abdullah University of Science and Technology (KAUST), 4700 KAUST, Thuwal 23955-6900, Kingdom of Saudi Arabia, E-mail: moussab.harb@kaust.edu.sa.

† Electronic Supplementary Information (ESI) available: [Cell parameters of Si, CdTe and GaAs computed using PBE and compared with available experimental data. Atomic positions of the constituting elements in the optimized β- and γ-VON structures]. See DOI: 10.1039/b000000x/

1 A. Shah, P. Torres, R. Tscharner, N. Wyrsch and H. Keppner, *Science* 1999, **285**, 692–698.
2 J. Nowotny, C. Sorrell, L. Sheppard and T. Bak, *Int. J. Hydrog. Energ.,* 2005, **30**, 521–544.
3 F. E. Osterloh, *Chem. Mater.,* 2008, **20**, 35–54.
4 M. Hernández-Alonso, F. Fresno, S. Suárez and J. M. Coronado, *Energ. Environ. Sci.,* 2009, **2**, 1231–1257.
5 A. Hadfeldt, G. Boschloo, L. Sun, L. Kloo and H. Pettersson, *Chem. Rev.,* 2010, **110**, 6595–6663.
6 R. R. Lunt, T. P. Osedach, P. R. Brown, J. A. Rowehl and V. Bulović, *Adv. Mater.,* 2011, **23**, 5712–5727.
7 O. Madelung, *Semiconductors: Data Handbook,* 3rd ed.; Springer: New York, 2004.
8 K. F. Young and H. P. R. Frederikse, *J. Phys. Chem. Ref. Data,* 1973, **2**, 313–409.
9 I. Pelant and J. Valenta, Luminescence of Excitons. In Luminescence Spectroscopy of Semiconductors; Oxford University Press: Oxford, U.K., 2012.
10 J. Zhang, T. Ruf, R. Lauck and M. Cardona, *Phys. Rev. B,* 1998, **57**, 9716–9722.
11 T. Taguchi, J. Shirafuji and Y. Inuishi, *Phys. Status Solidi b,* 1975, **68**, 727–738.

12 M. A. Gilleo, P. T. Bailey and D. E. Hill, *Phys. Rev.,* 1968, **174**, 898–905.
13 I. Vurgaftman, J. R. Meyer and L. R. Ram-Mohan, *J. Appl. Phys.,* 2001, **89**, 5815–5875.
14 S. Adashi, *GaAs and Related Materials;* World Scientific Publishing Co. Pte. Ltd.: Singapore, 1994.
15 M. Harb, P. Sautet and P. Raybaud, *J. Phys. Chem. C,* 2011, **115**, 19394–19404.
16 M. Harb, P. Sautet and P. Raybaud, *J. Phys. Chem. C,* 2013, **117**, 8892–8902.
17 M. Harb, *J. Phys. Chem. C,* 2013, **117**, 12942–12948.
18 M. Harb, *J. Phys. Chem. C,* 2013, **117**, 25229–25235.
19 M. Harb, D. Masih, S. Ould-Chikh, P. Sautet, J.-M. Basset and K. Takanabe, *J. Phys. Chem. C,* 2013, **117**, 17477–17484.
20 M. Harb, D. Masih and K. Takanabe, *Phys. Chem. Chem. Phys.,* 2014, **16**, 18198–18204.
21 M. Harb, P. Sautet, E. Nurlaela, P. Raybaud, L. Cavallo, K. Domen, J.-M. Basset and K. Takanabe, *Phys. Chem. Chem. Phys.,* 2014, **16**, 20548–20560.
22 M. Harb, L. Cavallo and J.-M. Basset, *J. Phys. Chem. C,* 2014, **118**, 20784–20790.
23 M. Harb, *J. Phys. Chem. C,* 2015, **119**, 4565–4572.
24 T. Le Bahers, M. Rérat and P. Sautet, *J. Phys. Chem. C,* 2014, **118**, 5997-6008.
25 D. Armytage and B. E. F. Fender, *Acta Crystallogr., Sect. B: Struct. Sci.,* 1974, **30**, 809–812.
26 H. Schilling, A. Stork, E. Irran, H. Wolff, T. Bredow, R. Dronskowski and M. Lerch, *Angew. Chem. Int. Ed.,* 2007, **46**, 2931–2934.
27 A. Neuhaus, *Chimia* 1964, **18**, 93–103.
28 G. Kresse and J. Hafner, *Phys. Rev. B,* 1994, **49**, 14251–14269.
29 G. Kresse and J. Furthmüller, *Phys. Rev. B,* 1996, **54**, 11169–11186.
30 G. Kresse and J. Furthmüller, *Comput. Mater. Sci.,* 1996, **6**, 15–50.
31 G. Kresse and D. Joubert, *Phys. Rev. B,* 1999, **59**, 1758–1775.
32 J. P. Perdew, K. Burke and M. Ernzerhof, *Phys. Rev. Lett.,* 1996, **77**, 3865–3868.
33 P. E. Blöchl, *Phys. Rev. B,* 1994, **50**, 17953–17979.
34 H. J. Monkhorst and J. D. Pack, *Phys. Rev. B,* 1976, **13**, 5188–5192.
35 M. R. Hoffmann, S. T. Martin, W. Choi and D. W. Bahnemann, *Chem. Rev.,* 1995, **95**, 69–96.
36 B. Delley, *J. Chem. Phys.,* 1990, **92**, 508–517.
37 J. Heyd, G. E. Scuseria and M. Ernzerhof, *J. Chem. Phys.,* 2003, **118**, 8207–8215.
38 S. Saha, T. P. Sinha and A. Mookerjee, *Phys. Rev. B,* 2000, **62**, 8828–8834.
39 M. Launay, F. Boucher and P. Moreau, *Phys. Rev. B,* 2004, **69**, 035101.
40 M. Gajdoš, K. Hummer, G. Kresse, J. Furthmüller and F. Bechstedt, *Phys. Rev. B,* 2006, **73**, 045112.
41 I. Souza, J. Iniguez and D. Vanderbilt, *Phys. Rev. Lett.,* 2002, **89**, 117602.
42 A. Fonari and C. Sutton, Effective Mass Calculator for Semiconductors, http://afonari.com/emc/.
43 A. Rodina, M. Dietrich, A. Göldner, L. Eckey, A. Hoffmann, A. Efros, M. Rosen and B. Meyer, *Phys. Rev. B,* 2001, **64**, 115204.